A window into transition metal availability in Early Palaeoproterozoic seawater

Ansahmbom Y. Nke[1], Rosalind E. M. Rickaby[2], Harilaos Tsikos[3], Paul R.D. Mason[4], Xolane Mhlanga[5], Rosalie Tostevin[1*]

[1]Department of Geological Sciences, University of Cape Town, Rondebosch, 7701, South Africa.

[2]Department of Earth Science, University of Oxford, Oxford, UK, OX1 3AN

[3]Department of Geology, University of Patras, Πανεπιστημιούπολη Πατρών 265 04, Greece.

[4]Department of Earth Sciences, Utrecht University, Princetonlaan 8a, 3584 CB Utrecht, Netherlands.

[5]School of Biology and Environmental Sciences, University of Mpumalanga, Mbombela, Mpumalanga, South Africa.

*Correspondence to rosalie.tostevin@uct.ac.za

1. CHARACTERISATION OF GREENALITE

1.1 X-ray diffraction (XRD)

Chert horizons within the Kuruman Formation that had a high likelihood of containing greenalite were targeted for bulk rock XRD analysis. Powder XRD samples, representing 1–2 cm of homogenized core material, were created using off-cuts from thin-sectioned samples. The off-cuts were crushed in a jaw crusher before being pulverized on a SIEBTECHNIK disk swing mill with a tungsten carbide steel mill set and rings at the University of Cape Town's (UCT's) Department of Geological Sciences. The identity of very fine-grained phases present in the powdered sample was determined using a Bruker AXS D8 Advanced X-ray diffractometer with a Co-anode and K radiation at the Chemical Engineering Department, UCT. The X-ray diffractometer was set to a generator voltage of 35 kV and a current of 40 mA, with 2θ values ranging from 5° to 120°. Data were collected in 0.031° 2θ step sizes, with the counting time set to 1 s for bulk powders. PANalytical X'Pert HighScore Plus software and PANalytical ICSD database were used for background stripping, indexing of diffraction peaks, and mineral identification. The peak position at 14.35° 2θ, with a d-spacing of 7.12 Å, is characteristic of greenalite (Fig. S1). The peaks were small compared to other minerals, such as quartz, ankerite, pyrite and minnesotaite, reflecting the relatively low abundance of greenalite in bulk iron formation.

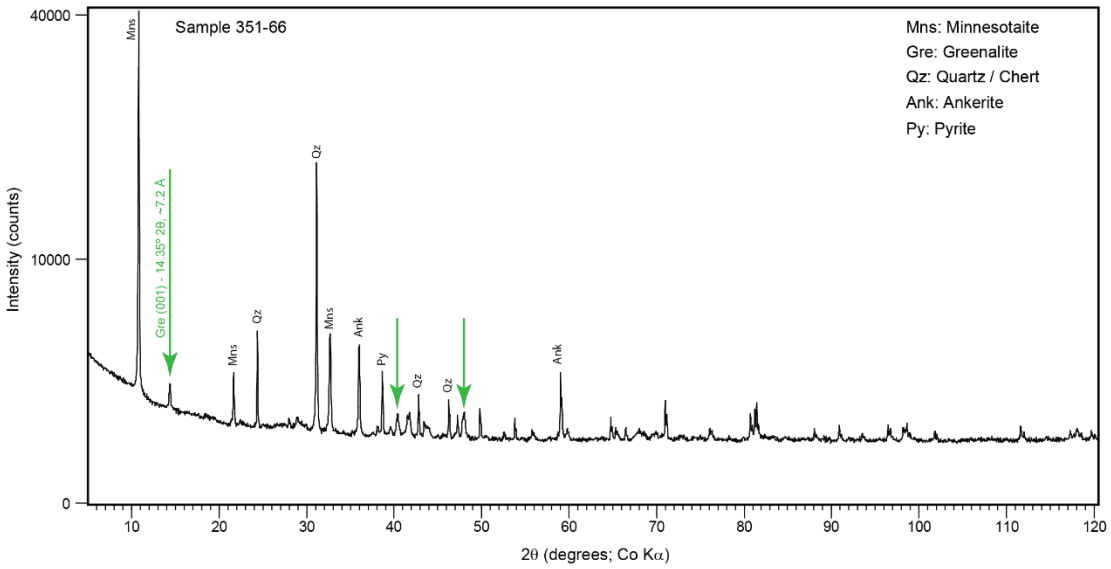

Fig. S1 | Representative bulk rock XRD pattern with greenalite peaks highlighted in green (7Å phase) and other phases shown in black (from ref. [1]).

1.2 Scanning electron microscopy-energy dispersive X-ray spectrometry (SEM-EDS)

Previous studies utilizing high-resolution imaging have identified greenalite as a primary phase in iron formations[2]. Building on this foundational work, our research aims to quantify the trace metal concentrations within greenalite. By coupling these measurements with established partition coefficients[3], we aim to infer the trace metal composition of seawater during the formation of this mineral phase. Critical to this analysis is the precise identification of greenalite and its extraction in quantities sufficient for laser ablation inductively coupled plasma mass spectrometry (LA-ICP-MS) analysis.

To achieve this, we inspected greenalite-bearing horizons further by creating stubs for SEM-EDS analysis. Greenalite laths were imaged in SEM-BSE and analysed for their chemical composition using SEM-EDS at the Chemical Engineering Department, UCT. The Nova NanoSEM at UCT was fitted with an Oxford Instruments XMax EDS, which was used for

quantitative and qualitative chemical analysis of mineral grains using AZtec software from Oxford Instruments. The samples were observed and imaged at a 5.5 mm working distance and 20 kV accelerating voltage.

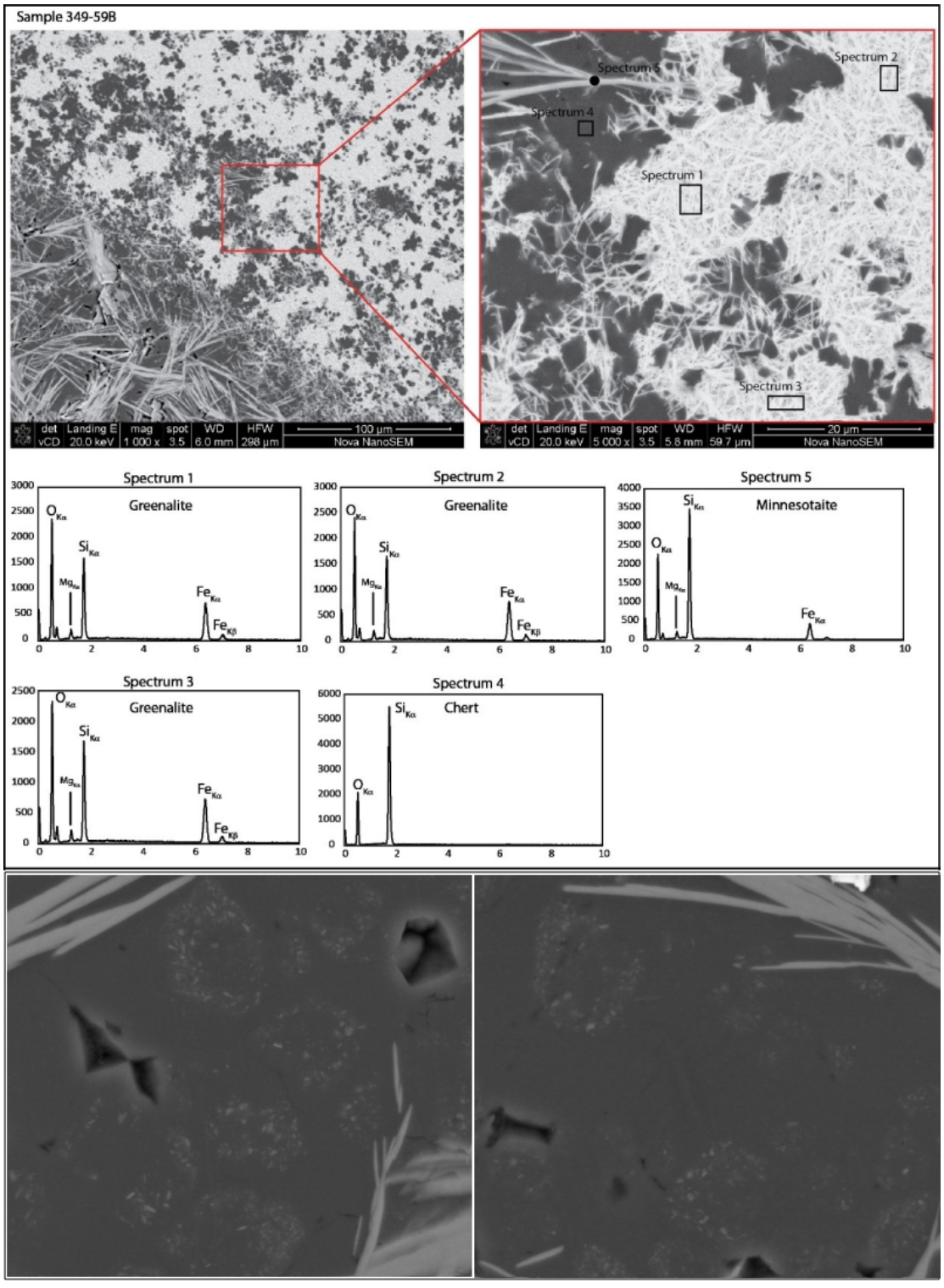

Fig. S2 | SEM-BSE images of greenalite-rich sample 349-59B, showing aggregates of greenalite (white) laths along with associated mineral phases (minnesotaite and chert) (**top**). The different phases are identified and distinguished using SEM-EDS spectra, generated at the areas highlighted in the top-right panel (**middle**). SEM-BSE images depicting characteristic polygonal microstructures formed by fine-grained greenalite laths within chert (**bottom**).

In drill core, the presence of greenalite imparts a dusty appearance and pale green coloration to chert. Internal lamination in very thinly laminated chert (typical laminae <1 mm thick) is commonly defined by greenalite. Greenalite is extremely fine-grained, occurring as laths, <1 μm in width and ~2–7 μm in length, which form dense aggregates (Fig. S2), which may represent clusters of nanoparticles that formed in the water column[2]. The most common greenalite assemblages are chert-calcite-minnesotaite-greenalite, chert-minnesotaite-greenalite, chert-greenalite, and occasionally chert-greenalite-siderite. In the chert-calcite-minnesotaite-greenalite assemblage, greenalite is cross-cut by calcite and is in turn crosscut by minnesotaite, suggesting that these grains did not form in equilibrium, and that greenalite was the earliest forming phase. Greenalite aggregates display smooth, sharp boundaries with other phases. Experimental work indicates that the primary phase precipitated from seawater was an amorphous Fe(II)-silicate gel, which crystallized to greenalite during heating and burial[4–6]. Since there is no direct evidence for this intermediate phase in the rock record, greenalite is referred to throughout this work. The reader is referred to ref. [1] for further details on the characteristics of greenalite.

1.3 Electron probe microanalysis (EPMA)

To confirm the identity of greenalite laths, further differentiating them from minnesotaite, we determined the major element composition of the Fe(II)-silicate phases using wavelength dispersive spectroscopy on the 5-spectrometer JEOL JXA-8530F Hyperprobe Electron Probe Micro-Analyser (EPMA) at Utrecht University (Fig. S3). The operational parameters include a 20 nA beam current and a 20 kV accelerating voltage. A defocused beam with a 10 µm diameter was used during EMPA analyses to capture the compositions of Fe-silicate phases. Calibration to natural mineral standards was performed, and the counting times for all elements were 20 seconds on peak and 10 seconds on background (see ref. [1] for the results of the EPMA analyses). EMPA analyses provided further confirmation of the identity of our targeted Fe(II)-silicate phases, revealing Si concentrations ranging from 15.0 to 18.4 wt.%, total Fe content ranging from 34.5 to 37.3 wt.%, characteristics consistent with greenalite (Fig. S3). Importantly, our findings demonstrate that these silicates are distinct from minnesotaite and other common Fe-silicates, despite potential geochemical similarities (Fig. S4).

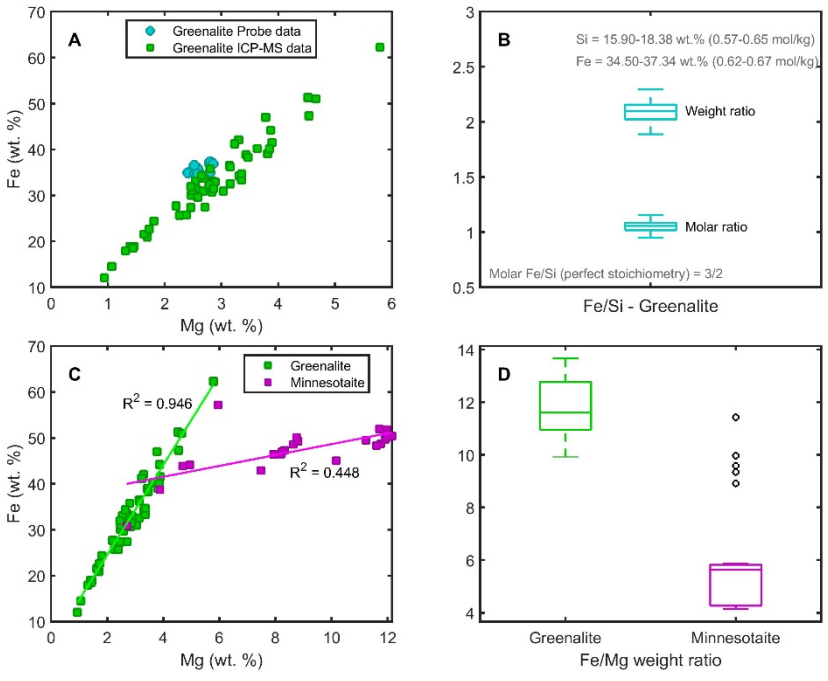

Fig. S3 | Microprobe and LA-ICP-MS major element data for greenalite in micro-banded IFs, Transvaal Supergroup, South Africa. A: Correlation between LA-ICP-MS and microprobe data. Both techniques yield comparable outcomes, with microprobe data exhibiting enhanced precision owing to its smaller beam size. B: Fe/Si weight and molar ratios assessment to confirm the identity of greenalite based on microprobe data. C & D: Distinguishing between our identified greenalite versus minnesotaite using LA-ICP-MS data. From ref. [1].

2. ESTIMATING GREENALITE-TO-CHERT PROPORTIONS

For each of the three samples, every laser crater represents an independent analysis of a unique group of greenalite laths within a single layer. Targeted laser craters contained both greenalite and chert, but a customized code written in MATLAB® (Mathworks Inc., Natick, MA, USA) was used to independently estimate the proportion of greenalite-to-chert around each laser ablation hole. The SEM-BSE images of laser ablation craters were used to identify regions that provided an accurate representation of mineral proportions (Fig. S4). The code involved image pre-processing, including isolating ROIs and smoothing the image. Selection of ROIs was based on the laser analysis spot size and the distribution of minerals closest to the ablated area. We employed Otsu's method[7] to automatically determine a global threshold for distinguishing chert and greenalite (dark and bright, respectively). This threshold was applied to segment the image into greenalite and chert, enabling the calculation of the proportions for each phase in the selected area (Fig. S4B). Colors, specifically white and grey, served as proxies for mineralogy in line with the greyscale nature of SEM-BSE images. It assumed a homogeneous average texture on a scale of 10–100 µm, and therefore the region around the crater is representative of the ablated area. The

majority of the spots contained >50% greenalite (see ref. [1] for the estimated mineral proportions).

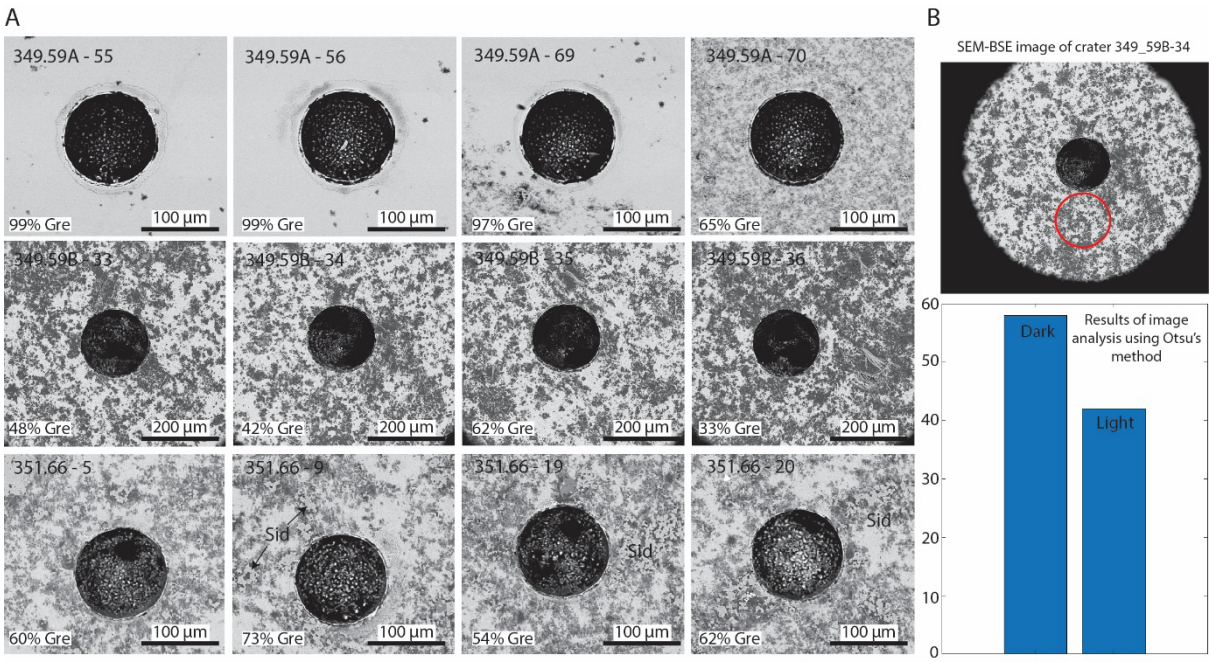

Fig. S4 | A: SEM-BSE micrographs of selected craters from in situ LA ICP-MS analyses on aggregates of greenalite laths, Transvaal Supergroup, South Africa, with 120 µm spot analyses. Greenalite appears white whereas chert is grey, and there are variable proportions of chert in each region. B: SEM-BSE image of a laser ablation crater showing a selected region (red circle) used to estimate the chert-to-greenalite proportion, alongside a histogram depicting the estimated proportion of greenalite (bright) to chert (dark) in the analysed area. From ref. [1].

3. EVALUATING THE MINERALOGICAL HOST FOR METALS

Our extensive characterisation of the mineralogy using XRD, SEM, and EPMA indicate that the only minerals present in the samples are greenalite, chert, and occasionally siderite. No additional minerals were identified in these layers via XRD or chemical analysis. While the

diameter of the laser and probe can be limiting for identifying very fine grained phases, no other phases, such as coatings on the surfaces of grains, were observed even under the highest resolution imaging. An important source of Mn in modern sediments is Mn-rich oxide coatings that form as grains and are transported through an oxygenated water column[8], but we would not expect these phases to form in the broadly anoxic Palaeoproterozoic oceans. Therefore, we assume that all metals detected via LA-ICP-MS are hosted in either greenalite or chert for samples 349-59A and 349-59B, and hosted in greenalite, chert, and siderite for 351-66.

We used bivariate plots of metal concentrations versus the proportion of greenalite for each analysed spot to confirm the metal-hosting associations (Fig. S5). The close correlation between the proportion of greenalite and the Co, V, Zn, and Ni content in samples 349-59A and 349-59B suggests that these metals are primarily hosted in greenalite, rather than chert (Fig. S5A-D). This is consistent with experimental data which show that these metals are associated with Fe(II)-silicate during precipitation and are retained in the structure during heating, which drives de-sorption of surface bound phases[4]. For at least one metal, Ni, synchrotron X-ray absorption spectroscopy data demonstrate that the metal is structurally incorporated in the octahedral sites[4]. This is strong evidence that these metals are incorporated into Fe(II)-silicate gel and are retained in the structure during transformation to crystalline greenalite. The relatively higher Ni concentrations in sample 351-66, and the lack of clear relationship between Ni content and % greenalite, suggests Ni can also be hosted in siderite[9].

Our data also show a close correlation between the proportion of greenalite and Mn content in samples 349-59A and 349-59B (Fig. S5E), suggesting Mn is also hosted in the

greenalite crystal. This is consistent with experimental work that demonstrates incorporation of Mn into the solid phase during precipitation[4]. The partition coefficient for Mn into Fe(II)-silicate is very low, consistent with the large ionic radii of Mn^{2+}, which sits on the upper limit of the range for greenalite (0.83 Å). Minor loss of Mn was observed during simulated diagenesis and crystallisation (<10%; ref. [4]). This suggests that although the majority of Mn is structurally incorporated, minor amounts could be surface-sorbed or associated with silica-coatings. Any loss of Mn during diagenesis could have reduced the primary Mn content of the greenalite in the Transvaal Supergroup, resulting in an underestimate of Mn concentrations in seawater. The relatively higher Mn concentrations in sample 351-66, and the lack of clear relationship between Mn content and % greenalite, suggests Mn is also hosted in siderite, as expected due to the close relationship between Mn and many carbonate group minerals[10].

Conversely, concentrations of Cu and Cd are notably higher in chert-rich samples, implying that they are *not* hosted in the greenalite crystal structure (Fig. S5F & G). Furthermore, experiments have shown that heating synthetic Fe(II)-silicate with silica sorped to the surface releases Cu (~20%) and Cd (~60%) alongside Si, which is also consistent with these metals being associated with surface bound phases, rather than Fe(II)-silicate[4,11]. Mo does not display any correlation with the proportion of greenalite, consistent with experiments which showed no uptake of Mo into the solid phase, and is unlikely to be hosted in greenalite (Fig. S5H). Cd, Cu, and Mo were therefore excluded from estimations of Archean seawater metal concentrations.

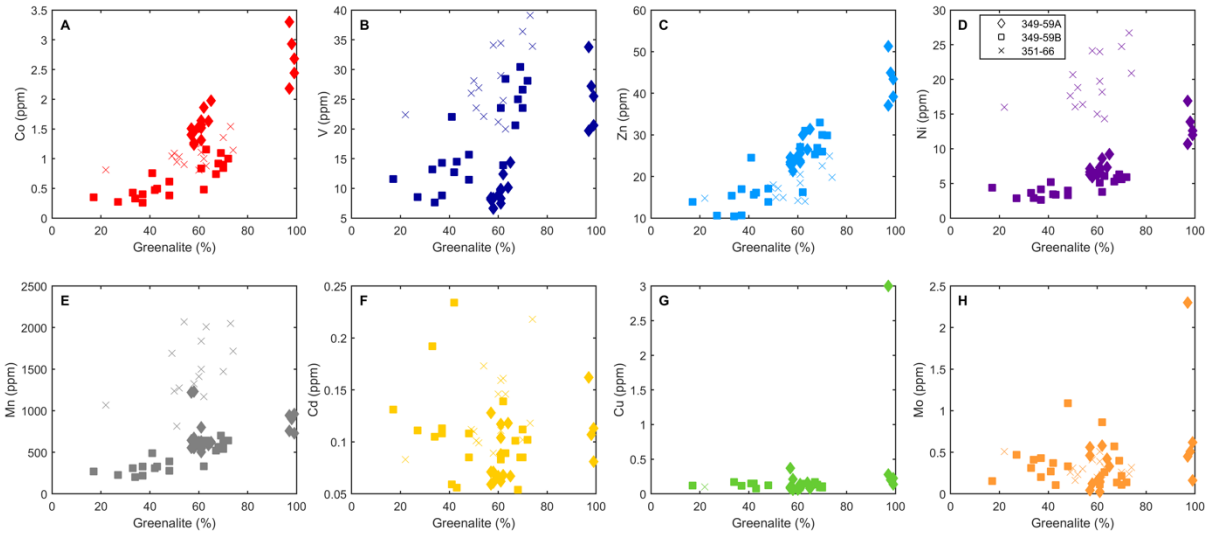

184

185 **Fig. S5 |** Bivariate plots of metal concentrations versus the proportion of greenalite for each

186 analysed spot to confirm the metal-hosting associations.

187

188 We compared our trace metal concentrations to published data from greenalite-chert from

189 the 2.483 Ga Colonial Chert Member of the Mount McRae Shale (2x sample Mitchell2-418)

190 and the 2.495–2.461 Ga Dales Gorge Member of the Brockman Iron Formation (2x sample

191 Mitch2-405C), Western Australia[12], and other greenalite-bearing horizons from the

192 Kuruman Formation of the Transvaal Supergroup[13]. The craters labelled "this study –

193 greenalite" in Fig. S6 contained > 50% greenalite (see section 2 above), while the craters

194 labelled "this-study - chert" in Fig. S6 contained 5–20 % greenalite, similar to those in the

195 Colonial chert (Mitchell2-418 = 5–28% Fe) and Dales Gorge Member greenalite-chert

196 (Mitch2-405C = 5.6–6.2% Fe). Notably, concentrations of V, Zn, Mo, Co, Ni, and Mn are

197 higher in our greenalite samples compared to those in Mitchell2-418 of Colonial chert and

198 Mitch2-405C of Dales Gorge Member greenalite-chert, which instead align more closely

199 align with our chert data (Fig. S6). These data support our inference that Cu, Cd, and Mo are

200 predominantly hosted in the chert phase.

201

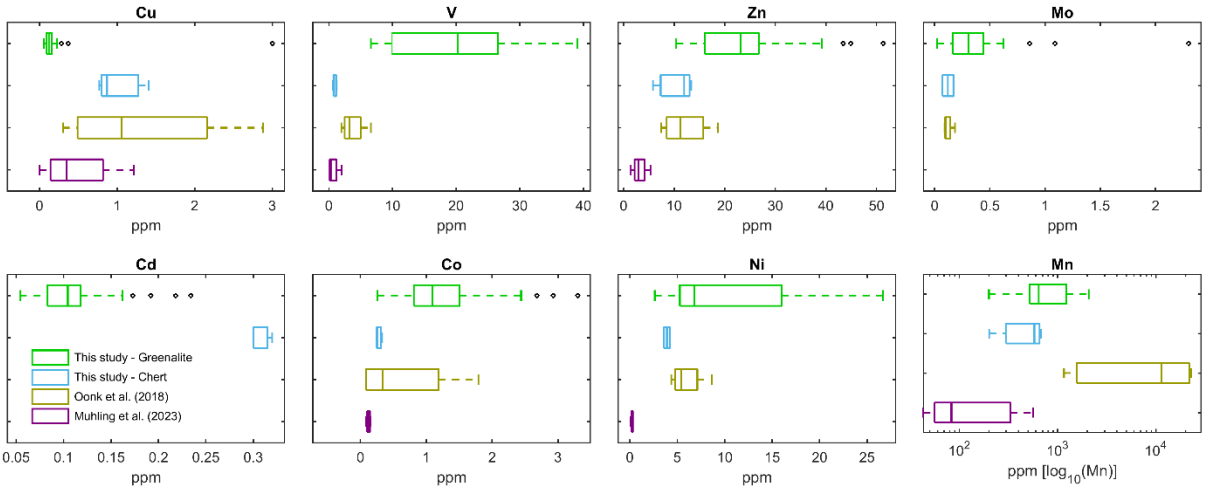

Fig. S6 | Comparison of our measured trace metal concentrations in Palaeoproterozoic, natural greenalite with the range of measured concentrations from other penecontemporaneous greenalite samples.

4. LOCATION OF GREENLITE PRECIPITATION

Our data reflect metal abundance in the local environment during the precipitation of greenalite which raises the question, where did these minerals form? Several potential pathways have been proposed for greenalite formation. One possibility is that greenalite was formed in and around hydrothermal vents from low pH, high temperature fluids. Models and experimental work both suggest that this pathway was feasible under predicted Palaeoproterozoic conditions[4,14,15], and this process could have shaped the metal fluxes from hydrothermal vents into bottom waters[4]. These minerals are preserved in exhalative deposits[15], and may have been transported and redeposited to shelf settings too[14]. Alternatively, greenalite precipitation could occur on the shelf, triggered by elevated temperatures, small increases in pH or the presence of small amounts of Fe^{3+}, which may be generated by warming, microbial activity or photo-oxidation reactions in shallow sunlit waters[5,16]. It is critical to determine the location of greenalite precipitation preserved in iron

220 formation to contextualise the metal data, because the metal content of hydrothermal
221 fluids is distinct from seawater. Recent rare earth element data suggests that the natural
222 greenalite from the Kuruman Formation, Transvaal Supergroup precipitated in a shelf
223 environment (see ref. [1] for more detailed discussions).
224
225 **REFERENCES**

226 1. Nke, A. Y., Tsikos, H., Mason, P. R., Mhlanga, X. & Tostevin, R. A seawater origin for
227 greenalite in iron formation. *Earth and Planetary Science Letters* **643**, 118917 (2024).
228 2. Rasmussen, B., Muhling, J. R. & Krapež, B. Greenalite and its role in the genesis of early
229 Precambrian iron formations–A review. *Earth-Science Reviews* **217**, 103613 (2021).
230 3. Tostevin, R. & Ahmed, I. A. M. Micronutrient availability in Precambrian oceans
231 controlled by greenalite formation. *Nat. Geosci.* **16**, 1188–1193 (2023).
232 4. Tostevin, R. & Ahmed, I. A. M. Micronutrient availability in Precambrian oceans
233 controlled by greenalite formation. *Nat. Geosci.* **16**, 1188–1193 (2023).
234 5. Hinz, I. L., Nims, C., Theuer, S., Templeton, A. S. & Johnson, J. E. Ferric iron triggers
235 greenalite formation in simulated Archean seawater. *Geology* **49**, 905–910 (2021).
236 6. Tosca, N. J., Guggenheim, S. & Pufahl, P. K. An authigenic origin for Precambrian
237 greenalite: Implications for iron formation and the chemistry of ancient seawater. *GSA*
238 *Bulletin* **128**, 511–530 (2016).
239 7. Otsu, N. A threshold selection method from gray-level histograms. *Automatica* **11**, 23–
240 27 (1975).
241 8. Balistrieri, L. S. & Murray, J. W. The surface chemistry of sediments from the Panama
242 Basin: The influence of Mn oxides on metal adsorption. *Geochimica et Cosmochimica*
243 *Acta* **50**, 2235–2243 (1986).

9. Dublet, G. *et al.* XAS evidence for Ni sequestration by siderite in a lateritic Ni-deposit from New Caledonia. *American Mineralogist* **99**, 225–234 (2014).
10. Sengupta, R., Tosca, N. J. & Robinson, S. A. Geochemical controls on the elemental composition of siderite: Implications for palaeo-environmental reconstructions. *Geochimica et Cosmochimica Acta* **271**, 1–15 (2020).
11. Tostevin, R. & Sevgen, S. The role of Fe (II)-silicate gel in the generation of Archean and Paleoproterozoic chert. *Geology* **52**, 706–711 (2024).
12. Muhling, J. R., Gilbert, S. E. & Rasmussen, B. Rare earth element and yttrium (REY) geochemistry of 3.46–2.45 Ga greenalite-bearing banded iron formations: New insights into iron deposition and ancient ocean chemistry. *Chemical Geology* **641**, 121789 (2023).
13. Oonk, P. B. H., Mason, P. R. D., Tsikos, H. & Bau, M. Fraction-specific rare earth elements enable the reconstruction of primary seawater signatures from iron formations. *Geochimica et Cosmochimica Acta* **238**, 102–122 (2018).
14. Tosca, N. J. & Tutolo, B. M. Hydrothermal vent fluid-seawater mixing and the origins of Archean iron formation. *Geochimica et Cosmochimica Acta* **352**, 51–68 (2023).
15. Rasmussen, B., Muhling, J. R. & Tosca, N. J. Nanoparticulate apatite and greenalite in oldest, well-preserved hydrothermal vent precipitates. *Sci. Adv.* **10**, eadj4789 (2024).
16. Rasmussen, B., Muhling, J. R., Suvorova, A. & Krapež, B. Greenalite precipitation linked to the deposition of banded iron formations downslope from a late Archean carbonate platform. *Precambrian Research* **290**, 49–62 (2017).